Atmos. Chem. Phys. Discuss., 15, 34765–34812, 2015
www.atmos-chem-phys-discuss.net/15/34765/2015/
doi:10.5194/acpd-15-34765-2015

Atmospheric Chemistry and Physics Discussions

Impact of the Asian monsoon on the extratropical lower stratosphere: trace gas observations during TACTS over Europe 2012

S. Müller[1], P. Hoor[1], H. Bozem[1], E. Gute[2,a], B. Vogel[3], A. Zahn[4], H. Bönisch[5], T. Keber[5], M. Krämer[3], C. Rolf[3], M. Riese[3], H. Schlager[6], and A. Engel[5]

[1]Institute for Atmospheric Physics, Johannes Gutenberg-University, Mainz, Germany
[2]Department of Atmospheric Chemistry, Max Planck Institute for Chemistry, Mainz, Germany
[3]Institute for Energy and Climate Research – Stratosphere (IEK-7), Forschungszentrum Jülich, Jülich, Germany
[4]Institute of Meteorology and Climate Research (IMK), Karlsruhe Institute of Technology (KIT), Karlsruhe, Germany
[5]Institute for Atmospheric and Environmental Sciences, Goethe-University of Frankfurt, Frankfurt am Main, Germany
[6]Institute for Atmospheric Physics, German Aerospace Research Center (DLR), Oberpfaffenhofen, Germany
[a]now at: Department of Chemistry, University of Toronto, Toronto, Canada

Received: 22 September 2015 – Accepted: 23 November 2015
– Published: 10 December 2015

Correspondence to: S. Müller (stefan.mueller@uni-mainz.de)

Published by Copernicus Publications on behalf of the European Geosciences Union.

ACPD
15, 34765–34812, 2015

Abstract

The transport of air masses originating from the Asian monsoon anticyclone into the extratropical upper troposphere and lower stratosphere (Ex-UTLS) above potential temperatures $\Theta = 380\,K$ was identified during the HALO aircraft mission TACTS in August and September 2012. In-situ measurements of CO, O_3 and N_2O during TACTS Flight 2 on the 30 August 2012 show the irreversible mixing of aged with younger (originating from the troposphere) stratospheric air masses within the Ex-UTLS. Backward trajectories calculated with the trajetory module of the CLaMS model indicate that these tropospherically affected air masses originate from the Asian monsoon anticyclone. From the monsoon circulation region these air masses are quasi-isentropically transported above $\Theta = 380\,K$ into the Ex-UTLS where they subsequently mix with stratospheric air masses. The overall trace gas distribution measured during TACTS shows that this transport pathway has a significant impact on the Ex-UTLS during boreal summer and autumn. This leads to an intensification of the tropospheric influence on the Ex-UTLS with $\Delta\Theta > 30\,K$ (relative to the tropopause) within three weeks during the TACTS mission. In the same time period a weakening of the tropospheric influence on the lowermost stratosphere (LMS) is determined. Therefore, the study shows that the transport of air masses originating from the Asian summer monsoon region within the lower stratosphere above $\Theta = 380\,K$ is of major importance for the change of the chemical composition of the Ex-UTLS from summer to autumn.

1 Introduction

The impact of air masses originating from the Asian monsoon anticyclone on the trace gas composition of the upper troposphere/lower stratosphere (UTLS) is not well known and therefore subject of current research (Dethof et al., 1999; Ploeger et al., 2013; Vogel et al., 2014, 2015; Park et al., 2007, 2008; Fadnavis et al., 2013, 2014, 2015). In general, the UTLS denotes the transition between the troposphere and the strato-

ACPD
15, 34765–34812, 2015

sphere (Gettelman et al., 2011). The tropopause, which suppresses exchange between the troposphere and stratosphere, is located within the UTLS region. In the tropics the UTLS is characterised by the slow diabatic ascent of air masses from the troposphere into the stratosphere within the Tropical Tropopause Layer (TTL) (Fueglistaler et al., 2009, and references therein). Contrary, diabatic cooling and descending air masses are typical for the stratospheric part of the Ex-UTLS (Holton et al., 1995). Within the Ex-UTLS the lowermost stratosphere (LMS) denotes the stratospheric part of the middle world (Hoskins et al., 1985), which is mainly characterised by exchange processes between the troposphere and stratosphere on time scales of days to weeks (Bönisch et al., 2009; Hoor et al., 2010). The LMS is vertically confined by the tropopause and potential temperatures Θ = 380 K (Holton et al., 1995) (or 400 K Hegglin and Shepherd, 2007). Above, the extratropical lower stratosphere (LS) is coupled with the tropical LS by the Brewer–Dobson-Circulation (BDC, Brewer, 1949; Dobson, 1956). The BDC consists of two significant different transport pathways. The deep branch of the BDC transports air from the tropics to the Ex-UTLS via the upper stratosphere and lower mesosphere on time scales of several years (Butchart, 2014). In contrast, the shallow branch links the tropical and extratropical stratosphere by quasi-isentropic transport and mixing with Θ between 380 and 450 K (Spackman et al., 2007; James and Legras, 2009; Birner and Bönisch, 2011).

A detailed knowledge of the relative strength of these transport pathways is of major importance to quantify the chemical composition of the Ex-UTLS, which in turn determines the radiative, dynamical and chemical impact of this atmospheric region on the climate system (Forster and Shine, 2002; Riese et al., 2012).

As shown in Bönisch et al. (2009) and Ploeger et al. (2013) the seasonality of stratospheric transport processes above Θ = 380 K leads to a seasonality of the chemical composition up to Θ = 430 K (the bottom of the tropical pipe) and a "flushing" of the lower stratosphere with young tropical air masses up to this level in summer and autumn (Hegglin and Shepherd, 2007). In this context, the Asian summer monsoon is an important pathway for the transport of tropospheric constituents into the stratosphere

ACPD
15, 34765–34812, 2015

and gains increasing attention in atmospheric research (Randel and Park, 2006; Randel et al., 2010; Park et al., 2007, 2008, 2009; Bergman et al., 2013; Fadnavis et al., 2013, 2014, 2015). Generally, the Asian summer monsoon consists of a cyclonic flow and convergence in the lower troposphere and a large scale anticyclonic circulation in the upper troposphere between June and September centered over southern Asia (Randel et al., 2010). This circulation pattern is coupled with persistent deep convection (Bourassa et al., 2012; Bergman et al., 2013), which lifts chemical constituents from the lower troposphere to the tropopause region and lower stratosphere. Therefore, water vapour and tropospheric trace gases as carbon monoxide (CO) and methane (CH_4) are relatively high within the Asian monsoon anticyclone (Rosenlof et al., 1997; Park et al., 2004, 2007), whereas ozone (O_3) is relatively low (Park et al., 2008). Since the monsoon tropopause is relatively high (Highwood and Hoskins, 1998), exchange processes between the troposphere and stratosphere in the region of the Asian monsoon may transport tropospheric constituents into the lower stratosphere to altitudes up to 20 km (Park et al., 2008). The pathway and strength of troposphere-to-stratosphere-transport (TST) in the tropopause region of the Asian monsoon are neither adequately understood nor quantified. In this context, the direct convective injection into the lower stratosphere (Rosenlof et al., 1997; Chen et al., 2012) and the seperation of small anticyclcones from the main anticyclone, so called "eddy shedding", is of major importance (Hsu and Plumb, 2000; Popovic and Plumb, 2001; Garny and Randel, 2013). The latter process can transport tropospheric trace gases and pollutants to mid- and high latitudes, where they mix with extratropical stratospheric air masses (Roiger et al., 2011; Vogel et al., 2014).

However, the impact of the Asian monsoon on the chemical composition of the northern hemispheric lower stratosphere cannot easily be seperated from the general upward transport of tropospheric air masses into the stratosphere in the tropics, which is regarded as the primary pathway for air masses entering the stratosphere (Holton et al., 1995). In the tropical lower stratosphere these ascending air masses are uplifted

ACPD
15, 34765–34812, 2015

by the Brewer–Dobson circulation and zonally transported to higher latitudes by the shallow branch of the BDC.

In this paper in-situ trace gas measurements of CO, nitrous oxide (N_2O), and O_3 in the Northern Hemisphere extratropical stratosphere up to potential temperatures $\Theta = 410$ K obtained during the TACTS (Transport and Composition in the Upper Troposphere and Lower Stratosphere) aircraft campaign are presented. Analysis data of the ECMWF (European Centre for Medium-Range Weather Forecast) and backward trajectories calculated with the trajectory module of the Chemical Lagrangian Model of the Stratosphere (CLaMS) (McKenna et al., 2002a, b; Konopka et al., 2010; Pommrich et al., 2014) are used for a more detailed interpretation of the measurements.

The focus is on the investigation of the quasi-isentropic transport of "young stratospheric" air masses from the (sub-)tropics into the Ex-UTLS in the lower stratosphere with $\Theta > 380$ K. "Young stratospheric" in this context denotes air masses, which are clearly located in the stratosphere with the respective stratospheric chemical composition, but which still exhibit chemical signatures of previous tropospheric influence (e.g. CO mixing ratios larger than the CO equilibrium mixing ratio of chemically processed (aged) stratospheric air masses of CO = 12.5 ± 2.5 ppbv (Herman et al., 1999; Flocke et al., 1999). Since the measurements were performed in boreal summer and autumn 2012 within a period of four weeks in a wide range of the northern hemispheric UTLS, the potential influence of the Asian monsoon on this transport pathway and therefore on the trace gas composition of Ex-UTLS is studied.

The paper is organised as follows: Sect. 2 gives an overview of the analysed measurements, model data, and backward trajectory calculations. Section 3 presents a case study of TACTS-Flight 2 (30 August 2012), which illustrates the identification of irreversible in-mixing of young stratospheric air masses into the Ex-UTLS above $\Theta = 380$ K. Tracer-tracer-scatterplots of TACTS-Flight 2 are analysed in Sect. 3.2. Section 3.3 shows the results of backward trajectory calculations, which indicate that transport and mixing from the Asian monsoon anticyclone into the Ex-UTLS cause the measured mixing event. Section 4 subsequently analyses the influence of the identi-

ACPD
15, 34765–34812, 2015

fied transport path on the trace gas distribution of the northern hemispheric Ex-UTLS during TACTS 2012. The investigation of the in-situ measured N_2O–O_3-scatterplot in Sect. 4.2 supports the before drawn conclusions. A summary and discussion of the results (Sect. 5) and a conclusion (Sect. 6) closes the paper.

2 Project overview, measurements, and backward trajectory calculation

2.1 The TACTS campaign 2012

In-situ measurements performed during the first atmospheric science mission with the new German research aircraft HALO in August/September 2012 named TACTS (Transport and Composition of the UTLS)/ESMVal (Earth System Model Vaildation) provide the basis for the presented study. During 13 mission flights with a duration between 8 and 10 h for each flight, a large dataset of high spatial and temporal resolution of mainly in-situ trace gas data was collected within the Ex-UTLS. This paper focuses on six research flights extending from 15 to 70° N and 25° W to 15° E. ESMVal Flight 7 (23 September 2012), which was performed in the same area, is additionally considered in the analysis. During these flights 65 h of measurement data in the Ex-ULTS were collected, including 40 h in the extratropical stratosphere.

The measurements of TACTS were examined during two phases. The inital phase with approx. 35 flights hours covered the time period between the 30 August and 5 September 2012. The end phase was performed from the 23 September until 26 September 2012. The time lag between both phases is used to investigate the seasonal variation of the trace gas composition of the Ex-UTLS in late summer and early autumn 2012 as shown in Sect. 4.

2.2 In-situ trace gas measurements

The study is mainly based on in-situ data from the TRIHOP (CO and N_2O) and FAIRO (O_3) instrument aboard HALO as described in the following subsections. Basic mete-

ACPD
15, 34765–34812, 2015

orological and avionic data are taken from the Basic HALO Measurement and Sensor System (BAHAMAS). For the following analysis all data are merged to one dataset with a time resolution of 10 s or 0.1 Hz, respectively, corresponding to a horizontal resolution of 2.5 km.

2.2.1 TRIHOP in-situ measurements of CO and N_2O

The TRIHOP instrument is a three channel Quantum Cascade Laser Infrared Absorption spectrometer capable of the subsequent measurement of CO, CO_2, and N_2O (Schiller et al., 2008). The instrument applies Quantum Cascade Laser Absorption Spectroscopy (QCLAS) in the mid-infrared with a multipass absorption cell (type White), which is kept at a constant pressure of $P = 30$ hPa and has a path length of 64 m and a volume of 2.7 L. During TACTS/ESMVal the instrument was in-situ calibrated approx. every 30 min during the flights against a secondary standard of compressed ambient air. The mixing ratios of the secondary standard were determined before and after the campaign in the laboratory against National Oceanic and Atmospheric Administration (NOAA) standards. Therefore, the in-flight calibrations allow to identify and correct slow instrumental drifts in the post-flight data evaluation. The integration time for each species was 1.5 s at a duty cycle of 8 s, which finally limits the temporal resolution of the measurements. During TACTS and ESMVal TRIHOP CO (N_2O) data achieved a 2σ precision of 1.0 (1.1) ppbv and stability of the instrument of 1.5 (2.2) ppbv, respectively, before applying the post flight data correction. Note that stability is based on the mean drift between two subsequent calibrations, which were performed in intervals of 30 min during the flights. These instrumental drifts are corrected after the flights assuming linear drift, which leads to a reduced uncertainty. Hence, the total uncertainty relative to the working standard of 1.8 (2.5) ppbv can be regarded as an upper limit.

ACPD
15, 34765–34812, 2015

2.2.2 FAIRO in-situ measurements of O_3

FAIRO is a new accurate ozone instrument developed for use on board the HALO aircraft. It combines two techniques, the UV photometry (light absorption of O_3 at λ = 250–260 nm) with high accuracy and chemiluminescence detection with high measurement frequency. A UV-LED is used as a light source for the UV photometer, which can be controlled well (in contrast to Hg lamps) for constant light emission. The 1σ precision is 0.08 ppbv at a measurement frequency of 4 s and a cuvette pressure of 1 bar and the total uncertainty is 2 %. The chemiluminescence detector shows a measurement frequency of 12.5 Hz and a precision of 0.05 ppbv (at 10 ppbv absolute, a measurement frequency of 5 Hz, and a pressure of 1 bar) (Zahn et al., 2012).

2.3 ECMWF (meteorological data)

Global meteorological analysis data (T1279L91) of the ECMWF (European Centre for Medium-Range Weather Forecast) are used to interpret the meteorological situation during TACTS Flight 2 as shown in Sect. 3.1. The meteorological fields are available every 3 h interpolated onto a regular grid of 0.5° horizontal spacing.

2.4 CLaMS-TRAJ (backward trajectories)

The trajectory module CLaMS-TRAJ of the Chemical Lagrangian Model for the Stratosphere (CLaMS) is used to calculate backward trajectories at the positions of the in-situ observations (McKenna et al., 2002a, b; Konopka et al., 2010; Pommrich et al., 2014). The trajectories are initialised every 10 s along the flight paths and calculated 50 days back in time. For this purpose ERA-Interim reanalysis data (Dee et al., 2011) with a resolution of 1° and 60 vertical levels from the surface up to 0.1 hPa are interpolated in time and space on the starting point of the backward trajectories. Meteorological data, e.g. pressure, temperature, altitude, Θ and potential vorticity (PV) are available every 1 h along the backward trajectories. The horizontal motion of the trajectories are

ACPD
15, 34765–34812, 2015

driven by horizontal winds from the ERA-Interim reanalysis data. For vertical motion the diabatic mode of CLaMS-TRAJ is used. Hereby diabatic heating rates are calculated as vertical velocities in the UTLS region for pressure levels lower than 300 hPa (Ploeger et al., 2010). Below $P > 300$ hPa a pressure-based hybrid vertical coordinate is applied (Pommrich et al., 2014).

3 Case study: TACTS Flight 2 on 30 August 2012

TACTS Flight 2 on 30 August 2012 was performed over western Europe and the eastern Atlantic with departure and landing in Oberpfaffenhofen near Munich (see Fig. 1). An eastward propagating trough over western Europa was crossed several times on pressure levels between 220 and 130 hPa equivalent to flight altitudes between 11.5 and 15 km. On the highest flight levels on 150 and 130 hPa, respectively, air masses with potential temperatures Θ between 380 and 410 K were sampled. Potential vorticity (PV) derived from ECMWF data are between 8 and 14 pvu for these flight sections (Fig. 1a and b). Hence, these air masses are located above the dynamical tropopause, which is typically defined by PV isolines between 1 and 4 pvu in the extratropics (Hoskins et al., 1985; Randel et al., 2007). In the subtropics above Θ = 340 K, PV at the tropopause varies between 2 and 5 pvu (Kunz et al., 2011).

3.1 Irreversible mixing within the stratosphere

The time series of in-situ O_3, CO and pressure data for TACTS Flight 2 are shown in Fig. 1c. The CO data indicates three sections with mixing ratios lower than 40 ppbv during the flight, which is below CO mixing ratios in the northern hemispheric free troposphere ranging from 50 to 130 ppbv (Kumar et al., 2013). This indicates that the respective flight sections were performed within the stratosphere. Accompanying $O_3 > 200$ ppbv (Strahan, 1999) and PV values larger than 5 pvu (cf. Fig. 1) support this conclusion.

ACPD
15, 34765–34812, 2015

During the last two flight segments from 10:30 until 12:15 UTC and 13:00 until 14:00 UTC, respectively, partly chemically processed stratospheric air masses with CO ranging from 20 to 30 ppbv were sampled. These values are larger than the stratospheric equilibrium of CO = 12.5 ± 2.5 ppbv (Herman et al., 1999; Flocke et al., 1999), which is reached by the CO degradation in the stratosphere on time scales of several months (Xiao et al., 2007). Therefore, CO between 20 and 30 ppbv indicates neither pure tropospheric nor completely CO degraded stratospheric air masses. Instead, mixing ratios in this range arise either due to irreversible mixing of tropospheric and stratospheric air masses or by the CO degradation of a former tropospheric air mass in the stratosphere (or a combination of both). In the following the correlation of CO with O_3 during TACTS Flight 2 is analysed to further examine the tropospheric influence in the Ex-UTLS for Θ between 380 and 410 K.

In general, without any exchange between the troposphere and stratosphere, the CO–O_3-scatterplot would form an L-shape (Fischer et al., 2000). Irreversible mixing of tropospheric (characterised by low O_3) and stratospheric (characterised by low CO) air masses appear as "mixing lines", which connect the mixed reservoirs on the tracer-tracer-scatterplot (Hoor et al., 2002). Previous studies used the method of mixing lines to investigate exchange processes between the troposphere and stratosphere within the extratropical tropopause layer (ExTL) (Zahn et al., 2000; Hoor et al., 2004; Pan, 2004). In this study in-situ observed mixing lines on the CO–O_3-scatterplot are used for the first time to investigate mixing and transport processes in the Ex-UTLS above Θ = 380 K.

Figure 2a shows the stratospheric part (O_3 > 200 ppbv) of the CO–O_3-scatterplot of TACTS Flight 2 color coded with potential temperature Θ. Low CO and high O_3 are accompanied by high values of Θ. From the fact that all CO data points are well above the stratospheric equilibrium of CO = 12.5±2.5 ppbv (Herman et al., 1999; Flocke et al., 1999), tropospheric influence on time scales of weeks can be deduced for all probed air masses. Additional, partly linear correlated data points with enhanced CO mixing ratios

ACPD
15, 34765–34812, 2015

on the generally curved correlation indicate recent irreversible transport of tropospheric air into the Ex-UTLS.

During TACTS Flight 2 five mixing lines (these mixing lines are in the following shortened with ML 1, 2, 4, 5) at potential temperatures $\Theta \geq 380$ K are identified. These are marked by individual colors in Fig. 2b. The respective colors in Fig. 1 mark the location of the measured mixing lines on the flight path (Fig. 1a and b) and along the time series of CO and O_3 (Fig. 1c). ML 1, 2, 4, 5 are measured in the center of the trough (Fig. 1a), ML 3 is sampled at the trough edge further south. The five identified mixing lines correspond to individual flight sections along the flight track with durations of typically 15 min for each mixing line (see Fig. 1c).

Table 1 lists the minimum and maximum values of CO, O_3 and Θ for each individual mixing line. Also shown are the number of data points, the flight distance, and R^2 from a linear fit regression for the respective mixing line. The applied fit is based on Press et al. (1992) and accounts for errors in both, x and y direction. The observed CO and O_3 variability of each mixing line larger 4 and 60 ppbv, respectively, is larger than the total measurement uncertainty of both species. Therefore, measurement artefacts that could yield these mixing lines can be excluded. $R^2 \geq 0.89$ indicates that linearity for all mixing lines is justified. In general, ML 3 is measured at larger CO and lower O_3 mixing ratios and exhibits a larger difference between the minimum and maximum values of both species compared to ML 1, 2, 4, 5. Especially significantly larger CO mixing ratios up to 40 ppbv compared to CO < 30 ppbv for ML 1, 2, 4, 5 indicate shorter time scales for the transport and mixing of CO rich air masses from the troposphere into the stratosphere for ML 3 compared to the other mixing events. The fact that ML 3 is measured at the trough edge and at lower potential temperatures compared to ML 1, 2, 4, 5 supports the assumption that different processes are responsible for the formation of ML 3 and ML 1, 2 4, 5. In the following section the origin of the CO enhanced air masses in the extratropical lower stratosphere is further investigated with N_2O as an additional in-situ measured trace gas.

ACPD
15, 34765–34812, 2015

3.2 Mixing line analysis

The analysis of mixing lines on tracer-tracer-scatter plots allows the determination of the initial mixing ratio of one trace gas, if the mixing ratio of the second trace gas before mixing is known (Hintsa et al., 1998; Hoor et al., 2002). However, in most cases the mixing ratios of both tracers before mixing are unknown. Therefore, a precise determination of the trace gas mixing ratio prior to the mixing event is usually not feasible. Nevertheless, mixing ratios just below the the tropopause of trace gases like O_3 and N_2O are fairly constant compared to their stratospheric gradient. Thus, the determination of the so called "tropospheric endmember" is possible with the above assumption. This is conducted for all mixing lines (see Sect. 3.1) based on the CO–O_3- and N_2O–CO-scatterplot. Figure 3 displays exemplarily the tropospheric endmember approximation for ML 4. The calculation of the shaded confidence region is based on the FITEXY-approach described by Press et al. (1992), which accounts for uncertainties in x and y direction. O_3 at the tropopause varies between 60 and 120 ppbv, with a seasonal cycle and regional variations as well. For the endmember approximation in this section a mixing ratio $O_{3\,\mathrm{Trop}}$ = 100 ppbv is applied, which is a reasonable value for the northern hemispheric summer (Zahn and Brenninkmeijer, 2003; Thouret et al., 2006). Alternatively, N_2O can be used to determine a tropospheric endmember. Superior to O_3, N_2O is inert in the troposphere and thus has an almost homogeneous distribution in the global troposphere. The sinks of N_2O are entirely in the stratosphere, which leads to a weak gradient of N_2O at the tropopause. Therefore, the N_2O mixing ratio at the tropopause is well defined, which makes N_2O an appropriate tracer for tropospheric air masses (Assonov et al., 2013; Müller et al., 2015). In August/September 2012 the free tropospheric mixing ratio of N_2O was 325 ± 0.5 ppbv, which is applied as N_2O_{Trop} (www.esrl.noaa.gov/gmd/hats/combined/N2O.html). Table 2 lists the potential range of the tropospheric endmember of CO from the calculated confidence region (shaded area in Fig. 3) for $O_{3\,\mathrm{Trop}}$ = 100 ppbv and N_2O_{Trop} = 325 ppbv, respectively. The results can be summarised as follows:

ACPD
15, 34765–34812, 2015

– The tropospheric endmembers of CO for ML 1, 2, 4, 5 are in a range from 35 to 55 ppbv. This is at the lower limit and even below typical tropospheric CO mixing ratios.

– Endmembers of CO based on the CO–O_3-correlation are different from the respective N_2O–CO-endmembers.

– CO endmembers between 55 and 70 ppbv for ML 3 includes typical mixing ratios at the tropopause, even though CO is at the lower limit for tropospheric CO mixing ratios.

A tropospheric endmember of CO below typical CO mixing ratios at the tropopause indicates that the respective mixing line is not the result of mixing between pure tropospheric and stratospheric air masses. (The term "pure" is used in this context to describe undiluted and chemically unprocessed, therefore not CO degraded, tropospheric air masses.) For those mixing lines the determined tropospheric CO endmembers do not describe the original CO mixing ratio of the unmixed air mass. Lower CO endmembers than found at the tropopause can only arise from the chemical degradation of CO in the stratosphere or previous mixing. Therefore, the observed mixing lines are the result of mixing between two stratospheric air masses with different age. Note that O_3 variability (and chemistry) in the lower stratosphere leads to differences in the tropospheric endmembers of CO based on the CO–O_3- and N_2O–O_3-correlation. Thus, the formation of ML 1, 2, 4, 5 can only be caused by the irreversible mixing of stratospheric air masses with different age. In contrast, ML 3 indicates the irreversible mixing of pure tropospheric and stratospheric air masses.

These findings are supported by the meteorological situation and location where the mixing lines were measured. Air masses that form ML 1, 2, 4, 5 are probed in the centre of the investigated trough far away from the jetstream (see Fig. 1). From the fact that strong convective activity cannot be identified in the measurement region during the flight, fast transport of pure tropospheric air masses up to $\Theta = 400$ K can be ruled out. ML 3 arises, in contrast to the other mixing lines, presumably as a consequence

ACPD
15, 34765–34812, 2015

of the irreversible mixing of pure tropospheric and stratospheric air masses at the jet stream, since this mixing event is measured at the edge of the trough in a region with high windspeed and windshear (Pan et al., 2006).

3.3 Results of backward trajectory calculations

In the following the origin of ML 1, 2, 4, 5, which were observed in the trough away from sharp isentropic PV gradients at the tropopause, are investigated. For this purpose 50 days backward trajectories are analysed. These were calculated with the trajectory module of the CLaMS-model according to Sect. 2.4. Variations of potential temperature Θ along the backward trajectories indicate diabatic processes in the history of the respective probed air masses. Figure 4 shows the measured Θ along TACTS Flight 2 (30 August 2012) color coded with PV from ECMWF analysis data. Black dots indicate the maximum potential temperature along each individual backward trajectory. These values are typically 20 K higher than the measured Θ. This is in accordance with descending air masses in the extratropical stratosphere with a rate of approx. 0.5 K day^{-1} (Butchart, 2014). Red dots indicate the minimum Θ for trajectories which show a diabatic ascent from their origin at $t_{\mathrm{Tra}} < -50$ days prior to the time of measurement. These trajectories appear preferably for probed air masses with relatively large PV > 8 pvu in regions with the observed mixing lines from the previous sections. This finding provides an indication that diabatic upward transport of tropospherically influenced air masses in the measurement region is visible in the calculated backward trajectories. Figure 5 displays those trajectories, which show a significant diabatic increase exceeding 5 K. These trajectories indicate an origin in the anticyclone of the Asian summer monsoon and subsequent transport to the measurement region in the Ex-UTLS above Θ = 400 K. The position of the respective trajectories for -50 days $< t_{\mathrm{Tra}} < -30$ days in Fig. 6 shows that almost all trajectories are located within the Asian monsoon anticyclone for $t_{\mathrm{Tra}} < -30$ days. The lowest potential temperatures along the trajectories (bluish colors) appear within the Asian monsoon region.

ACPD
15, 34765–34812, 2015

The backward trajectory calculation suggest that diabatic ascent within the Asian monsoon transports tropospherically influenced air masses up to altitudes between 16 and 18 km. Figure 7 shows that this process is accompanied by PV values rising above 5 pvu and Θ larger 400 K. These air masses are subsequently transported at $t \approx -30$ days to the extratropics were they mix with aged stratospheric air masses (as measured).

The calculation of 50 days backward trajectories cannot provide unambiguous evidence that the transport of air masses from the Asian monsoon into the Ex-UTLS causes the occurence of mixing lines on the CO–O_3-correlation. However, as mentioned before, CLaMS allows to calculate the vertical motion using diabatic heating rates from ERA-Interim, which tend to have a relatively small vertical dispersion in the stratosphere compared to kinematic scenarios (Ploeger et al., 2010). Notably, Vogel et al. (2014) show that 40 days backward trajectories, calculated with the same setup of CLaMS as used in this study, agree with trace gas measurements during TACTS Flight 6.

In this study, trace gas measurements of TACTS Flight 2 and 50 days backward trajectories are consistent, since:

- CO–O_3 mixing lines indicate mixing at $\Theta > 380$ K. Endmember analysis shows that recent mixing at the tropopause cannot explain these mixing lines. The mixed air masses rather have experienced a significant CO degradation in the stratosphere. CLaMS trajectory calculations confirm this conclusion, since a transport time of $t \approx 30$ days from the Asian monsoon region into the Ex-UTLS is indicated by the backward trajectories.

- Figure 8 shows that the filtered backward trajectories belong to data points on the CO–O_3-correlation, which are located in the region of the identified mixing lines.

The only trajectories that indicate transport from the troposphere into the Ex-UTLS above $\Theta = 380$ K originate from the Asian monsoon region. A significant contribution from the TTL for this region for TACTS Flight 2 cannot be identified based on the tra-

ACPD
15, 34765–34812, 2015

jectory calculations. Thus, it is concluded that the Asian monsoon affects the trace gas composition of the Ex-UTLS for $\Theta > 380\,K$ during TACTS Flight 2. Subsequently, the overall trace gas distribution of the Ex-UTLS measured during TACTS 2012 is investigated in the following section. It will be discussed, if the boreal Ex-UTLS during August and September 2012 is affected by air masses originating from the Asian monsoon region.

4 Seasonality of N_2O, CO and O_3 during TACTS 2012

4.1 Trace gas distribution and variability of N_2O, CO and O_3

The effect of the Asian monsoon on the overall trace gas composition in the Ex-UTLS during August and September 2012 is investigated. Therefore, the trace gas distribution of N_2O, CO and O_3 from the initial (28 August to 5 September 2012) and final (23 to 26 September 2012) stage of TACTS, and the mixing ratio differences of both time periods, are displayed in a potential temperature Θ – equivalent latitude ϕ_{eq} – coordinate system in Fig. 10. The data coverage of each bin for both periods is shown in Fig. 9.

As can be seen from Fig. 10, no significant changes for the long-lived trace gases N_2O and O_3 during the flight campaign within the ExTL are evident. Above the ExTL with $\Delta\Theta > 30\,K$ (relative to the tropopause Strahan et al., 2007) an increase in N_2O during TACTS is observed. O_3 exhibits lower values for the same region during the final phase of the measurements. Both indicates an increasing impact of tropospheric air masses in the extratropical stratosphere above the ExTL. This finding is also valid for the distribution of the relatively short-lived species CO, which displays slightly larger mixing ratios above the ExTL. Within the ExTL a decrease of CO during the campaign occurs. These findings are interpreted as follows:

– Lower CO in the ExTL indicates a weakening of the tropospheric influence in the ExTL during TACTS between August und September 2012. This is not detectable

ACPD
15, 34765–34812, 2015

in the long lived tracers N_2O and O_3 due to the long chemical lifetime of both trace gases in the lowermost stratosphere.

– Above the ExTL, the transport of relatively young air masses within the stratosphere at $\Theta > 380$ K is responsible for larger mixing ratios of tropospheric (N_2O and CO) and lower mixing ratios of stratospheric tracers (O_3) in the Ex-UTLS. At mid- and high-latitudes these air masses subsequently descend to lower potential temperatures.

– If the transport of air masses from the troposphere below $\Theta = 380$ K into the stratosphere on short time scales was responsible for the enhancement of tropospheric signatures above the ExTL, larger CO in the ExTL would be appearent.

Both results are in accordance with previous studies regarding the Ex-UTLS region (Hoor et al., 2002, 2004, 2010; Bönisch et al., 2009). At this point it is hypothesized that the intensification of the jet stream during autumn is responsible for a weaker transport of tropospheric air masses into the ExTL (Haynes and Shuckburgh, 2000; Berthet et al., 2007; Sawa et al., 2008), which subsequently leads to lower CO mixing ratios at the final stage of the TACTS measurements. Independently from this transport pathway, the transport of Asian monsoon influenced air masses (as measured during TACTS Fligth 2) by the shallow branch of the Brewer–Dobson-circulation above $\Theta = 400$ K leads to a stronger tropospheric influence above the ExTL.

To further investigate this, the full 50 day backward trajectory data set is analysed in Fig. 11. Hereby the relative proportion of trajectories originating from the Asian monsoon region (criterion: 20° N < TRA-latitude < 50° N, 40° E < TRA-longitude < 150° E and Tra-$\Theta > 360$ K at $t = -30$ days) is displayed in the same coordinate system as the trace gas distributions in the top array of Fig. 11. The mean residence time of the filtered trajectories in the region of the Asian monsoon between $t = 0$ and -50 days is shown in the bottom array of Fig. 11.

Trajectories for data points within the ExTL predominantly originate from the Asian monsoon region during the initial phase of TACTS. Above the ExTL, trajectories orig-

ACPD
15, 34765–34812, 2015

inating from the monsoon anticyclone are preferably found for data points during the final stage of TACTS. The mean residence time of those trajectories within the Asian monsoon anticyclone shows no significant difference for both regions and time periods. These results clearly indicate that the Asian monsoon has impacted the Ex-UTLS during TACTS 2012. Further, the calculated trajectories give additional evidence that the measured increased tropospheric influence in the extratropical lower stratosphere arises due to air masses from the Asian monsoon region. Less trajectories originating from the Asian monsoon for the later measurements within ExTL indicate, in accordance to lower CO mixing ratios, a stronger transport barrier between the tropical troposphere and extratropical stratosphere.

4.2 The N_2O–O_3 correlation

The previous section shows that the composition of the extratropical lower stratosphere has significantly changed from late August to September 2012. As shown in Hegglin et al. (2006), Hegglin and Shepherd (2007) and Bönisch et al. (2011), the seasonality of transport affects the correlation between O_3 and N_2O. More O_3 relative to N_2O indicates a stronger contribution from the tropical production region of O_3 and thus tropical influence, whereas in winter diabatic downwelling from the stratosphere leads to a decrase of O_3 relative to N_2O. Therefore, an increased tropical and Asian monsoon influence should also affect the N_2O correlation in the same way by increasing O_3 relative to N_2O. If this assumption is correct, the overall N_2O–O_3-correlation should inherently contain the information on the composition change during TACTS 2012. Relatively large O_3 mixing ratios on a given N_2O level should be related to a more tropical or monsoonal origin, thus be encountered rather during the late TACTS phase. Lower O_3 levels relative to N_2O are indicative for a stronger contribution of descending chemically processed stratospheric air masses in the Ex-UTLS. Such air masses in the extratropical lower stratosphere were predominantly measured during the early phase of TACTS.

ACPD
15, 34765–34812, 2015

To test this, the lower stratospheric N_2O–O_3 correlation was subdivided in a low and high O_3 part. Fig. 12a displays the N_2O–O_3 scatter plot of all northern hemispheric data points of TACTS 2012 filtered for air masses of the lowermost stratosphere with $O_3 > 350$ ppbv. The respective parts of the correlation were analysed according to the time when measured. Figure 12b shows the histogram of the time of measurement of the blue and red points in Fig. 12a. Significantly more tropically influenced air masses were measured in the later phase of TACTS. This indicates an increasing influence of air masses from the tropical (or Asian monsoon) in the extratropical lower stratosphere during TACTS 2012.

Additional histograms for trace gas mixing ratios for extratropical (red) and tropical (blue) data points of SF_6, H_2O and total water ($2CH_4 + H_2O$) in Fig. 13 support this conclusion. SF_6 exhibits larger mixing ratios for blue data points. This indicates a younger age of air for the later phase of the measurements (Bönisch et al., 2009). Larger total water and water vapour mixing ratios are detected predominantly in the later TACTS phase. For the season investigated, tropical stratospheric air masses at and above $\Theta = 400$ K exhibit larger H_2O mixing ratios compared to mid- and high latitudes (Ploeger et al., 2013). Globally the highest water vapour mixing ratios at $\Theta = 390$ K occur in the region of monsoonal circulations (Randel and Jensen, 2013). Therefore, larger water vapour and total water mixing ratios indicate a stronger impact of tropical or monsoonal influenced air masses.

Larger CO mixing ratios on O_3-isopleths for the later observations in Fig. 14 are also indicative for an increasing tropospheric influence in the Ex-UTLS during TACTS. These results show that the measured N_2O–O_3 correlation also contains the finding of a strengthening influence of the Asian monsoon (or tropics) on the Ex-UTLS above $\Theta = 380$ K during TACTS 2012.

ACPD
15, 34765–34812, 2015

5 Discussion and summary

The measurements and backward trajectories provide a coherent picture, indicating a significant influence of the Asian summer monsoon on the Ex-UTLS over europe during TACTS 2012. A combination of methods is applied to obtain reliability in the stated conclusion, which can be summarized as follows:

Section 3:

1. Based on in-situ trace gas measurements, irreversible mixing of different air masses in the Ex-UTLS above $\Theta = 380$ K was observed during TACTS 2012.

2. The tropospheric endmember approximation shows that the observed irreversible mixing occured between air masses of different stratospheric ages rather than between tropospheric and stratospheric air masses.

3. Backward trajectories indicate that the younger of the mixed stratospheric air masses were affected by the Asian monsoon circulation.

Section 4:

4. An effect of the Asian monsoon on the LS over europe is also evident from the overall trace gas distributions measured during TACTS 2012. These show that the Ex-UTLS composition over Europe significantly changes within 20–30 days during the campaign. Above the ExTL a stronger impact of tropospherically influenced air masses in late September compared to late August 2012 is determined by larger CO and N_2O, and lower O_3 mixing ratios. Above the tropopause within the ExTL a weakening of the tropospheric influence is indicated by decreasing CO.

5. Backward trajectories originating from the Asian monsoon region for data points measured in the lowermost stratosphere predominantly appear during the late phase of TACTS 2012. Within the ExTL such trajectories are preferably found during the initial phase of the campaign.

ACPD
15, 34765–34812, 2015

6. The analysis of the N_2O–O_3-correlation shows an increasing impact of "younger" stratospheric air masses in the extratropical lower stratosphere during TACTS, which originate from the tropics or monsoonal regions.

The presented study indicates that the transport of air masses from the Asian monsoon region into the extratropical stratosphere is a major driver of the modification of the Ex-UTLS chemical composition during summer and autumn of the Northern Hemisphere (Hoor et al., 2005; Hegglin and Shepherd, 2007; Bönisch et al., 2009). Thereby, a significant increase of the tropospheric impact in the extratropical lower stratosphere within a few weeks (above the ExTL) is observed with in-situ data of N_2O, CO and O_3. This finding shows that also other atmospheric constituents within the Ex-UTLS beside water vapour (Ploeger et al., 2013; Randel and Jensen, 2013) are affected by the Asian monsoon circulation.

The presented case study indicates that air masses originating from the Asian monsoon are quasi-isentropically transported above $\Theta = 380$ K into the Ex-ULTS. This confirms the results of model calculations and satellite data of Ploeger et al. (2013), which show an enhanced water vapour transport from the tropics (and the Asian monsoon region into the extratropics during boreal summer above $\Theta = 380$ K. A relatively large effective diffusivity between the tropics and extratropics during summer and autumn for Θ between 380 and 450 K is also in accordance to the results of the presented study (Haynes and Shuckburgh, 2000).

Further, Haynes and Shuckburgh (2000) calculate a decreasing effective diffusivity from summer to autumn for Θ between 350 and 370 K (13–15 km), which indicates an increasing transport barrier from the early to the late monsoon season at the jet location. The measurement of lower CO within the ExTL during the later phase of TACTS compared to the initial phase agrees with a stronger transport barrier for mixing across the tropopause below $\Theta = 380$ K. In accordance, Ploeger et al. (2015) diagnose on the basis of the PV-gradient a strong transport barrier that seperates the anticyclone from its surrounding and inhibits isentropic transport and mixing between $\Theta = 360$–380 K. Our measurements also support the hypothesis of an efficient transport of tro-

ACPD
15, 34765–34812, 2015

pospheric trace gases (e.g. CO) to the upper Asian monsoon troposphere (Bergman et al., 2013). From there a significant ratio of these air masses is efficently transported and mixed into the lower stratosphere of mid- and high-latitudes at potential temperatures $\Theta > 380$ K (Berthet et al., 2007). Thus, our data shows that the Asian summer monsoon significantly affects the overall tracer distribution over Europe with increasing efficiency from August to September 2012.

6 Conclusions

In-situ measurements of CO, O_3 and N_2O during TACTS 2012 show a significant change of the trace gas composition over the course of four weeks in the Ex-UTLS up to $\Theta = 410$ K. From August to late September 2012 a significant increase of N_2O and CO (and decrease O_3) indicate a stronger tropospheric contribution above the ExTL up to $\Theta = 410$ K. Decreasing CO mixing ratios in the ExTL below $\Theta = 370$ K indicate a weakening of the quasi-isentropic transport across the tropopause at the jetstream into the lowermost stratosphere (Pan et al., 2006). Therefore, it is concluded that the observed increase of the tropospheric fraction above the ExTL is not caused by quasi-isentropic cross tropopause transport at the jetstream. Rather, the observed increase of tropospheric contribution must have originated in a region with a high tropopause. The calculation of 50 days backward trajectories with CLaMS-TRAJ shows that the Asian summer monsoon significantly influences the composition of the Ex-UTLS during TACTS 2012. In agreement with the tracer observations these trajectories indicate an increasing fraction of air masses originating from the Asian summer monsoon in the extratropical lower stratosphere from August to September 2012. Notably, the trajectories exhibit a mean residence time of $t > 200$ h in the Asian monsoon anticyclone in the last 50 days before the measurements. Within the monsoon circulation the trajectories slowly rise up to $\Theta > 400$ K. As shown in a case study in Sect. 3, the monsoonally influenced air masses are transported to the measurement region within 30 days. For the global tracer distribution increasing SF_6 values for the late phase of the measurements

ACPD
15, 34765–34812, 2015

consistently indicate an increase of younger air in agreement with the analysis of the backward trajectories. Further, the simultaneously observed increase of (total) water vapour for the same air masses is in accordance with the horizontal tape recorder of H_2O at $\Theta = 390\,K$ caused by the Asian monsoon (Randel and Jensen, 2013). Thus, the Asian summer monsoon significantly contributes to the observed "flushing" of the boreal extropical lower stratosphere from summer to autumn (Hegglin and Shepherd, 2007) when the tropospheric signature is at maximum (Hoor et al., 2005; Bönisch et al., 2009).

Acknowledgements. Thanks go to Michael Sprenger and Heini Wernli for the calculation of tropopause informations and providing ECMWF data. Further we thank Horst Fischer for helpful discussions and comments on the manuscript and for providing the TRIHOP instrument. Also the technical support before and during the TACTS campaign by Uwe Parchatka and Rainer Königstedt is acknowledged. Particulary we thank the flight department of the DLR, especially the pilots, for execution of the flights. We also thank the University of Mainz for financial support of the experiments. Flight planning for the TACTS/ESMVal campaign was assisted with CLaMS model forecasts, supported by the German Research Foundation (DFG) through project LASSO (HALO-SPP 1294/GR3786).

References

Assonov, S., Brenninkmeijer, C., Schuck, T., and Umezawa, T.: N_2O as a tracer of mixing stratospheric and tropospheric air based on CARIBIC data with applications for CO_2, Atmos. Environ., 79, 769–779, doi:10.1016/j.atmosenv.2013.07.035, 2013. 34777

Bergman, J. W., Fierli, F., Jensen, E. J., Honomichl, S., and Pan, L. L.: Boundary layer sources for the Asian anticyclone: regional contributions to a vertical conduit, J. Geophys. Res.-Atmos., 118, 2560–2575, doi:10.1002/jgrd.50142, 2013. 34769, 34787

Berthet, G., Esler, J. G., and Haynes, P. H.: A Lagrangian perspective of the tropopause and the ventilation of the lowermost stratosphere, J. Geophys. Res., 112, D18102, doi:10.1029/2006JD008295, 2007. 34782, 34787

Birner, T. and Bönisch, H.: Residual circulation trajectories and transit times into the extratropical lowermost stratosphere, Atmos. Chem. Phys., 11, 817–827, doi:10.5194/acp-11-817-2011, 2011. 34768

Bönisch, H., Engel, A., Curtius, J., Birner, Th., and Hoor, P.: Quantifying transport into the lowermost stratosphere using simultaneous in-situ measurements of SF_6 and CO_2, Atmos. Chem. Phys., 9, 5905–5919, doi:10.5194/acp-9-5905-2009, 2009. 34768, 34782, 34784, 34786, 34788

Bönisch, H., Engel, A., Birner, Th., Hoor, P., Tarasick, D. W., and Ray, E. A.: On the structural changes in the Brewer–Dobson circulation after 2000, Atmos. Chem. Phys., 11, 3937–3948, doi:10.5194/acp-11-3937-2011, 2011. 34783

Bourassa, A. E., Robock, A., Randel, W. J., Deshler, T., Rieger, L. A., Lloyd, N. D., Llewellyn, E. J., and Degenstein, D. A.: Large volcanic aerosol load in the stratosphere linked to Asian monsoon transport, Science, 337, 78–81, doi:10.1126/science.1219371, 2012. 34769

Brewer, A. W.: Evidence for a world circulation provided by the measurements of helium and water vapour distribution in the stratosphere, Q. J. Roy. Meteor. Soc., 75, 351–363, doi:10.1002/qj.49707532603, 1949. 34768

Butchart, N.: The Brewer–Dobson circulation, Rev. Geophys., 52, 157–184, doi:10.1002/2013RG000448, 2014. 34768, 34779

Chen, B., Xu, X. D., Yang, S., and Zhao, T. L.: Climatological perspectives of air transport from atmospheric boundary layer to tropopause layer over Asian monsoon regions during boreal summer inferred from Lagrangian approach, Atmos. Chem. Phys., 12, 5827–5839, doi:10.5194/acp-12-5827-2012, 2012. 34769

Dee, D. P., Uppala, S. M., Simmons, A. J., Berrisford, P., Poli, P., Kobayashi, S., Andrae, U., Balmaseda, M. A., Balsamo, G., Bauer, P., Bechtold, P., Beljaars, A. C. M., van de Berg, L., Bidlot, J., Bormann, N., Delsol, C., Dragani, R., Fuentes, M., Geer, A. J., Haimberger, L., Healy, S. B., Hersbach, H., Hólm, E. V., Isaksen, L., Kållberg, P., Köhler, M., Matricardi, M., McNally, A. P., Monge-Sanz, B. M., Morcrette, J.-J., Park, B.-K., Peubey, C., de Rosnay, P., Tavolato, C., Thépaut, J.-N., and Vitart, F.: The ERA-Interim reanalysis: configuration and performance of the data assimilation system, Q. J. Roy. Meteor. Soc., 137, 553–597, doi:10.1002/qj.828, 2011. 34773

ACPD
15, 34765–34812, 2015

Dethof, A., O'Neill, A., Slingo, J. M., and Smit, H. G. J.: A mechanism for moistening the lower stratosphere involving the Asian summer monsoon, Q. J. Roy. Meteor. Soc., 125, 1079–1106, doi:10.1002/qj.1999.49712555602, 1999. 34767

Dobson, G. M. B.: Origin and distribution of the polyatomic molecules in the atmosphere, Proc. R. Soc. Lon. Ser.-A., 236, 187–193, 1956. 34768

Fadnavis, S., Semeniuk, K., Pozzoli, L., Schultz, M. G., Ghude, S. D., Das, S., and Kakatkar, R.: Transport of aerosols into the UTLS and their impact on the Asian monsoon region as seen in a global model simulation, Atmos. Chem. Phys., 13, 8771–8786, doi:10.5194/acp-13-8771-2013, 2013. 34767, 34769

Fadnavis, S., Schultz, M. G., Semeniuk, K., Mahajan, A. S., Pozzoli, L., Sonbawne, S., Ghude, S. D., Kiefer, M., and Eckert, E.: Trends in peroxyacetyl nitrate (PAN) in the upper troposphere and lower stratosphere over southern Asia during the summer monsoon season: regional impacts, Atmos. Chem. Phys., 14, 12725–12743, doi:10.5194/acp-14-12725-2014, 2014. 34767, 34769

Fadnavis, S., Semeniuk, K., Schultz, M. G., Kiefer, M., Mahajan, A., Pozzoli, L., and Sonbawane, S.: Transport pathways of peroxyacetyl nitrate in the upper troposphere and lower stratosphere from different monsoon systems during the summer monsoon season, Atmos. Chem. Phys., 15, 11477–11499, doi:10.5194/acp-15-11477-2015, 2015. 34767, 34769

Fischer, H., Wienhold, F. G., Hoor, P., Bujok, O., Schiller, C., Siegmund, P., Ambaum, M., Scheeren, H. A., and Lelieveld, J.: Tracer correlations in the northern high latitude lowermost stratosphere: influence of cross-tropopause mass exchange, Geophys. Res. Lett., 27, 97–100, doi:10.1029/1999GL010879, 2000. 34775

Flocke, F., Herman, R. L., Salawitch, R. J., Atlas, E., Webster, C. R., Schauffler, S. M., Lueb, R. A., May, R. D., Moyer, E. J., Rosenlof, K. H., Scott, D. C., Blake, D. R., and Bui, T. P.: An examination of chemistry and transport processes in the tropical lower stratosphere using observations of long-lived and short-lived compounds obtained during STRAT and POLARIS, J. Geophys. Res.-Atmos., 104, 26625–26642, doi:10.1029/1999JD900504, 1999. 34770, 34775

Forster, P. D. de F. and Shine, K. P.: Assessing the climate impact of trends in stratospheric water vapor, Geophys. Res. Lett., 29, 10–14, doi:10.1029/2001GL013909, 2002. 34768

Fueglistaler, S., Dessler, A. E., Dunkerton, T. J., Folkins, I., Fu, Q., and Mote, P. W.: Tropical tropopause layer, Rev. Geophys., 47, RG1004, doi:10.1029/2008RG000267, 2009. 34768

ACPD
15, 34765–34812, 2015

Garny, H. and Randel, W. J.: Dynamic variability of the Asian monsoon anticyclone observed in potential vorticity and correlations with tracer distributions, J. Geophys. Res.-Atmos., 118, 13421–13433, doi:10.1002/2013JD020908, 2013. 34769

Gettelman, A., Hoor, P., Pan, L. L., Randel, W. J., Hegglin, M. I., and Birner, T.: The extratropical upper troposphere and lower stratosphere, Rev. Geophys., 49, RG3003, doi:10.1029/2011RG000355, 2011. 34768

Haynes, P. and Shuckburgh, E.: Effective diffusivity as a diagnostic of atmospheric transport: 2. Troposphere and lower stratosphere, J. Geophys. Res.-Atmos., 105, 22795–22810, doi:10.1029/2000JD900092, 2000. 34782, 34786

Hegglin, M. I. and Shepherd, T. G.: O_3-N_2O correlations from the atmospheric chemistry experiment: revisiting a diagnostic of transport and chemistry in the stratosphere, J. Geophys. Res., 112, D19301, doi:10.1029/2006JD008281, 2007. 34768, 34783, 34786, 34788

Hegglin, M. I., Brunner, D., Peter, T., Hoor, P., Fischer, H., Staehelin, J., Krebsbach, M., Schiller, C., Parchatka, U., and Weers, U.: Measurements of NO, NO_y, N_2O, and O_3 during SPURT: implications for transport and chemistry in the lowermost stratosphere, Atmos. Chem. Phys., 6, 1331–1350, doi:10.5194/acp-6-1331-2006, 2006. 34783

Herman, R. L., Webster, C. R., May, R. D., Scott, D. C., Hu, H., Moyer, E. J., Wennberg, P. O., Hanisco, T. F., Lanzendorf, E. J., Salawitch, R. J., Yung, Y. L., Margitan, J. J., and Bui, T. P.: Measurements of CO in the upper troposphere and lower stratosphere, Chemosph. – Glob. Chang. Sci., 1, 173–183, doi:10.1016/S1465-9972(99)00008-2, 1999. 34770, 34775

Highwood, E. J. and Hoskins, B. J.: The tropical tropopause, Q. J. Roy. Meteor. Soc., 124, 1579–1604, doi:10.1002/qj.49712454911, 1998. 34769

Hintsa, E. J., Boering, K. A., Weinstock, E. M., Anderson, J. G., Gary, B. L., Pfister, L., Daube, B. C., Wofsy, S. C., Loewenstein, M., Podolske, J. R., Margitan, J. J., and Bui, T. P.: Troposphere-to-stratosphere transport in the lowermost stratosphere from measurements of H_2O, CO_2, N_2O and O_3, Geophys. Res. Lett., 25, 2655–2658, doi:10.1029/98GL01797, 1998. 34777

Holton, J. R., Haynes, P. H., McIntyre, M. E., Douglass, A. R., Rood, R. B., and Pfister, L.: Stratosphere-troposphere exchange, Rev. Geophys., 33, 403–439, doi:10.1029/95RG02097, 1995. 34768, 34769

Hoor, P., Fischer, H., Lange, L., Lelieveld, J., and Brunner, D.: Seasonal variations of a mixing layer in the lowermost stratosphere as identified by the CO-O_3 correlation from in situ mea-

ACPD
15, 34765–34812, 2015

surements, J. Geophys. Res.-Atmos., 107, ACL 1–1–ACL 1–11, doi:10.1029/2000JD000289, 2002. 34775, 34777, 34782
Hoor, P., Gurk, C., Brunner, D., Hegglin, M. I., Wernli, H., and Fischer, H.: Seasonality and extent of extratropical TST derived from in-situ CO measurements during SPURT, Atmos. Chem. Phys., 4, 1427–1442, doi:10.5194/acp-4-1427-2004, 2004. 34775, 34782
Hoor, P., Fischer, H., and Lelieveld, J.: Tropical and extratropical tropospheric air in the lowermost stratosphere over Europe: a CO-based budget, Geophys. Res. Lett., 32, L07802, doi:10.1029/2004GL022018, 2005. 34786, 34788
Hoor, P., Wernli, H., Hegglin, M. I., and Bönisch, H.: Transport timescales and tracer properties in the extratropical UTLS, Atmos. Chem. Phys., 10, 7929–7944, doi:10.5194/acp-10-7929-2010, 2010. 34768, 34782
Hoskins, B. J., McIntyre, M. E., and Robertson, A. W.: On the use and significance of isentropic potential vorticity maps, Q. J. Roy. Meteor. Soc., 111, 877–946, doi:10.1002/qj.49711147002, 1985. 34768, 34774
Hsu, C. J. and Plumb, R. A.: Nonaxisymmetric thermally driven circulations and upper-tropospheric monsoon dynamics, J. Atmos. Sci., 57, 1255–1276, doi:10.1175/1520-0469(2000)057<1255:NTDCAU>2.0.CO;2, 2000. 34769
James, R. and Legras, B.: Mixing processes and exchanges in the tropical and the subtropical UT/LS, Atmos. Chem. Phys., 9, 25–38, doi:10.5194/acp-9-25-2009, 2009. 34768
Konopka, P., Grooß, J.-U., Günther, G., Ploeger, F., Pommrich, R., Müller, R., and Livesey, N.: Annual cycle of ozone at and above the tropical tropopause: observations versus simulations with the Chemical Lagrangian Model of the Stratosphere (CLaMS), Atmos. Chem. Phys., 10, 121–132, doi:10.5194/acp-10-121-2010, 2010. 34770, 34773
Kumar, A., Wu, S., Weise, M. F., Honrath, R., Owen, R. C., Helmig, D., Kramer, L., Val Martin, M., and Li, Q.: Free-troposphere ozone and carbon monoxide over the North Atlantic for 2001–2011, Atmos. Chem. Phys., 13, 12537–12547, doi:10.5194/acp-13-12537-2013, 2013. 34774
Kunz, A., Konopka, P., Müller, R., and Pan, L. L.: Dynamical tropopause based on isentropic potential vorticity gradients, J. Geophys. Res., 116, D01110, doi:10.1029/2010JD014343, 2011. 34774
McKenna, D. S., Grooß, J.-U., Günther, G., Konopka, P., Müller, R., Carver, G., and Sasano, Y.: A new Chemical Lagrangian Model of the Stratosphere (CLaMS) 2. Formulation of

ACPD
15, 34765–34812, 2015

chemistry scheme and initialization, J. Geophys. Res.-Atmos., 107, ACH 4-1–ACH 4-14, doi:10.1029/2000JD000113, 2002a. 34770, 34773

McKenna, D. S., Konopka, P., Grooß, J.-U., Günther, G., Müller, R., Spang, R., Offermann, D., and Orsolini, Y.: A new Chemical Lagrangian Model of the Stratosphere (CLaMS) 1. Formulation of advection and mixing, J. Geophys. Res.-Atmos., 107, ACH 15-1–ACH 15-15, doi:10.1029/2000JD000114, 2002b. 34770, 34773

Müller, S., Hoor, P., Berkes, F., Bozem, H., Klingebiel, M., Reutter, P., Smit, H. G. J., Wendisch, M., Spichtinger, P., and Borrmann, S.: In situ detection of stratosphere-troposphere exchange of cirrus particles in the midlatitudes, Geophys. Res. Lett., 42, 949–955, doi:10.1002/2014GL062556, 2015. 34777

Pan, L. L.: Definitions and sharpness of the extratropical tropopause: a trace gas perspective, J. Geophys. Res., 109, D23103, doi:10.1029/2004JD004982, 2004. 34775

Pan, L. L., Konopka, P., and Browell, E. V.: Observations and model simulations of mixing near the extratropical tropopause, J. Geophys. Res., 111, D05106, doi:10.1029/2005JD006480, 2006. 34779, 34787

Park, M., Randel, W. J., Kinnison, D. E., Garcia, R. R., and Choi, W.: Seasonal variation of methane, water vapor, and nitrogen oxides near the tropopause: satellite observations and model simulations, J. Geophys. Res.-Atmos., 109, D03302, doi:10.1029/2003JD003706, 2004. 34769

Park, M., Randel, W. J., Gettelman, A., Massie, S. T., and Jiang, J. H.: Transport above the Asian summer monsoon anticyclone inferred from aura microwave limb sounder tracers, J. Geophys. Res., 112, D16309, doi:10.1029/2006JD008294, 2007. 34767, 34769

Park, M., Randel, W. J., Emmons, L. K., Bernath, P. F., Walker, K. A., and Boone, C. D.: Chemical isolation in the Asian monsoon anticyclone observed in Atmospheric Chemistry Experiment (ACE-FTS) data, Atmos. Chem. Phys., 8, 757–764, doi:10.5194/acp-8-757-2008, 2008. 34767, 34769

Park, M., Randel, W. J., Emmons, L. K., and Livesey, N. J.: Transport pathways of carbon monoxide in the Asian summer monsoon diagnosed from Model of Ozone and Related Tracers (MOZART), J. Geophys. Res.-Atmos., 114, D08303, doi:10.1029/2008JD010621, 2009. 34769

Ploeger, F., Konopka, P., Günther, G., Grooß, J.-U., and Müller, R.: Impact of the vertical velocity scheme on modeling transport in the tropical tropopause layer, J. Geophys. Res., 115, D03301, doi:10.1029/2009JD012023, 2010. 34774, 34780

ACPD
15, 34765–34812, 2015

Ploeger, F., Günther, G., Konopka, P., Fueglistaler, S., Müller, R., Hoppe, C., Kunz, A., Spang, R., Grooß, J.-U., and Riese, M.: Horizontal water vapor transport in the lower stratosphere from subtropics to high latitudes during boreal summer, J. Geophys. Res.-Atmos., 118, 8111–8127, doi:10.1002/jgrd.50636, 2013. 34767, 34768, 34784, 34786

Ploeger, F., Gottschling, C., Griessbach, S., Grooß, J.-U., Günther, G., Konopka, P., Müller, R., Riese, M., Stroh, F., Ungermann, J., Vogel, B., and von Hobe, M.: A PV-based determination of the transport barrier in the Asian summer monsoon anticyclone, Atmos. Chem. Phys. Discuss., 15, 10593–10628, doi:10.5194/acpd-15-10593-2015, 2015. 34786

Pommrich, R., Müller, R., Grooß, J.-U., Konopka, P., Ploeger, F., Vogel, B., Tao, M., Hoppe, C. M., Günther, G., Spelten, N., Hoffmann, L., Pumphrey, H.-C., Viciani, S., D'Amato, F., Volk, C. M., Hoor, P., Schlager, H., and Riese, M.: Tropical troposphere to stratosphere transport of carbon monoxide and long-lived trace species in the Chemical Lagrangian Model of the Stratosphere (CLaMS), Geosci. Model Dev., 7, 2895–2916, doi:10.5194/gmd-7-2895-2014, 2014. 34770, 34773, 34774

Popovic, J. M. and Plumb, R. A.: Eddy shedding from the upper-tropospheric Asian monsoon anticyclone, J. Atmos. Sci., 58, 93–104, doi:10.1175/1520-0469(2001)058<0093:ESFTUT>2.0.CO;2, 2001. 34769

Press, W., Teukolsky, S., Vetterling, W., Flannery, B., and Yudin, V.: Numerical Recipes: The Art of Scientific Computing, 2nd edn., Cambridge Univ. Press, Cambridge, New York, 1992. 34776, 34777, 34801

Randel, W. J. and Jensen, E. J.: Physical processes in the tropical tropopause layer and their roles in a changing climate, Nat. Geosci., 6, 169–176, doi:10.1038/ngeo1733, 2013. 34784, 34786, 34788

Randel, W. J. and Park, M.: Deep convective influence on the Asian summer monsoon anticyclone and associated tracer variability observed with Atmospheric Infrared Sounder (AIRS), J. Geophys. Res.-Atmos., 111, D12314, doi:10.1029/2005JD006490, 2006. 34769

Randel, W. J., Seidel, D. J., and Pan, L. L.: Observational characteristics of double tropopauses, J. Geophys. Res., 112, D07309, doi:10.1029/2006JD007904, 2007. 34774

Randel, W. J., Park, M., Emmons, L., Kinnison, D., Bernath, P., Walker, K. A., Boone, C., and Pumphrey, H.: Asian monsoon transport of pollution to the stratosphere, Science, 328, 611–613, doi:10.1126/science.1182274, 2010. 34769

ACPD
15, 34765–34812, 2015

Riese, M., Ploeger, F., Rap, A., Vogel, B., Konopka, P., Dameris, M., and Forster, P.: Impact of uncertainties in atmospheric mixing on simulated UTLS composition and related radiative effects, J. Geophys. Res., 117, D16305, doi:10.1029/2012JD017751, 2012. 34768

Roiger, A., Schlager, H., Schäfler, A., Huntrieser, H., Scheibe, M., Aufmhoff, H., Cooper, O. R., Sodemann, H., Stohl, A., Burkhart, J., Lazzara, M., Schiller, C., Law, K. S., and Arnold, F.: In-situ observation of Asian pollution transported into the Arctic lowermost stratosphere, Atmos. Chem. Phys., 11, 10975–10994, doi:10.5194/acp-11-10975-2011, 2011. 34769

Rosenlof, K. H., Tuck, A. F., Kelly, K. K., Russell, J. M., and McCormick, M. P.: Hemispheric asymmetries in water vapor and inferences about transport in the lower stratosphere, J. Geophys. Res.-Atmos., 102, 13213–13234, doi:10.1029/97JD00873, 1997. 34769

Sawa, Y., Machida, T., and Matsueda, H.: Seasonal variations of CO_2 near the tropopause observed by commercial aircraft, J. Geophys. Res.-Atmos., 113, D23301, doi:10.1029/2008JD010568, 2008. 34782

Schiller, C. L., Bozem, H., Gurk, C., Parchatka, U., Königstedt, R., Harris, G. W., Lelieveld, J., and Fischer, H.: Applications of quantum cascade lasers for sensitive trace gas measurements of CO, CH_4, N_2O and HCHO, Appl. Phys. B, 92, 419–430, doi:10.1007/s00340-008-3125-0, 2008. 34772

Spackman, J. R., Weinstock, E. M., Anderson, J. G., Hurst, D. F., Jost, H.-J., and Schauffler, S. M.: Aircraft observations of rapid meridional transport from the tropical tropopause layer into the lowermost stratosphere: implications for midlatitude ozone, J. Geophys. Res.-Atmos., 112, D12308, doi:10.1029/2006JD007618, 2007. 34768

Strahan, S. E.: Climatologies of lower stratospheric NO_y and O_3 and correlations with N_2O based on in situ observations, J. Geophys. Res., 104, 30463, doi:10.1029/1999JD900775, 1999. 34774

Strahan, S. E., Duncan, B. N., and Hoor, P.: Observationally derived transport diagnostics for the lowermost stratosphere and their application to the GMI chemistry and transport model, Atmos. Chem. Phys., 7, 2435–2445, doi:10.5194/acp-7-2435-2007, 2007. 34781

Thouret, V., Cammas, J.-P., Sauvage, B., Athier, G., Zbinden, R., Nédélec, P., Simon, P., and Karcher, F.: Tropopause referenced ozone climatology and inter-annual variability (1994–2003) from the MOZAIC programme, Atmos. Chem. Phys., 6, 1033–1051, doi:10.5194/acp-6-1033-2006, 2006. 34777

Vogel, B., Günther, G., Müller, R., Grooß, J.-U., Hoor, P., Krämer, M., Müller, S., Zahn, A., and Riese, M.: Fast transport from Southeast Asia boundary layer sources to northern Europe:

ACPD
15, 34765–34812, 2015

rapid uplift in typhoons and eastward eddy shedding of the Asian monsoon anticyclone, Atmos. Chem. Phys., 14, 12745–12762, doi:10.5194/acp-14-12745-2014, 2014. 34767, 34769, 34780

Vogel, B., Günther, G., Müller, R., Grooß, J.-U., and Riese, M.: Impact of different Asian source regions on the composition of the Asian monsoon anticyclone and on the extratropical lowermost stratosphere, Atmos. Chem. Phys. Discuss., 15, 9941–9995, doi:10.5194/acpd-15-9941-2015, 2015. 34767

WMO: Meteorology – A Three-dimensional Science, WMO Bull., 6, 134–138, 1957. 34807, 34808

Xiao, Y., Jacob, D. J., and Turquety, S.: Atmospheric acetylene and its relationship with CO as an indicator of air mass age, J. Geophys. Res.-Atmos., 112, D12305, doi:10.1029/2006JD008268, 2007. 34775

Zahn, A. and Brenninkmeijer, C. A. M.: New directions: a chemical tropopause defined, Atmos. Environ., 37, 439–440, 2003. 34777

Zahn, A., Brenninkmeijer, C. A. M., Maiss, M., Scharffe, D. H., Crutzen, P. J., Hermann, M., Heintzenberg, J., Wiedensohler, A., Güsten, H., Heinrich, G., Fischer, H., Cuijpers, J. W. M., and van Velthoven, P. F. J.: Identification of extratropical two-way troposphere-stratosphere mixing based on CARIBIC measurements of O_3, CO, and ultrafine particles, J. Geophys. Res.-Atmos., 105, 1527–1535, doi:10.1029/1999JD900759, 2000. 34775

Zahn, A., Weppner, J., Widmann, H., Schlote-Holubek, K., Burger, B., Kühner, T., and Franke, H.: A fast and precise chemiluminescence ozone detector for eddy flux and airborne application, Atmos. Meas. Tech., 5, 363–375, doi:10.5194/amt-5-363-2012, 2012. 34773

ACPD
15, 34765–34812, 2015

Table 1. Minimum and maximum values of potential temperature, and CO and O_3 mixing ratios, respectively, for every mixing line. Additonally the number of data points, the flight distance, and R^2 based on a linear regression is listed.

Mixing line	Line 1	Line 2	Line 3	Line 4	Line 5
Θ_{min} [K]	381.5	385.3	377.0	399.0	396.5
Θ_{max} [K]	384.5	389.0	382.0	405.0	401.0
CO_{min} [ppbv]	23.4	23.9	23.7	21.9	23.5
CO_{max} [ppbv]	27.4	28.7	41.4	28.7	28.0
$O_{3\,min}$ [ppbv]	425.59	421.75	248.27	467.82	433.01
$O_{3\,max}$ [ppbv]	485.56	495.11	377.92	583.16	493.54
Date points	71	71	60	65	51
Flight distance [km]	142	142	120	130	102
R^2	0.96	0.96	0.99	0.89	0.96

ACPD
15, 34765–34812, 2015

Table 2. Tropospheric "endmembers" for every mixing line based on the tracer-tracer-correlations of O_3 and CO, and N_2O and CO, respectively (cf. Fig. 3). The values are based on the intercept between the calculated confidence regions with the assumed mixing ratio of O_3 and N_2O at the tropopause in Fig. 3.

Mixing line	Line 1	Line 2	Line 3	Line 4	Line 5
$R_{Trop}(O_3) = 100$ ppbv					
CO_{min} [ppbv]	42.0	45.9	59.3	47.2	44.5
CO_{max} [ppbv]	50.9	52.7	62.2	54.0	55.1
$R_{Trop}(N_2O) = 325$ ppbv					
CO_{min} [ppbv]	35.1	35.4	54.1	38.8	35.2
CO_{max} [ppbv]	44.2	39.8	68.0	46.2	47.3

ACPD
15, 34765–34812, 2015

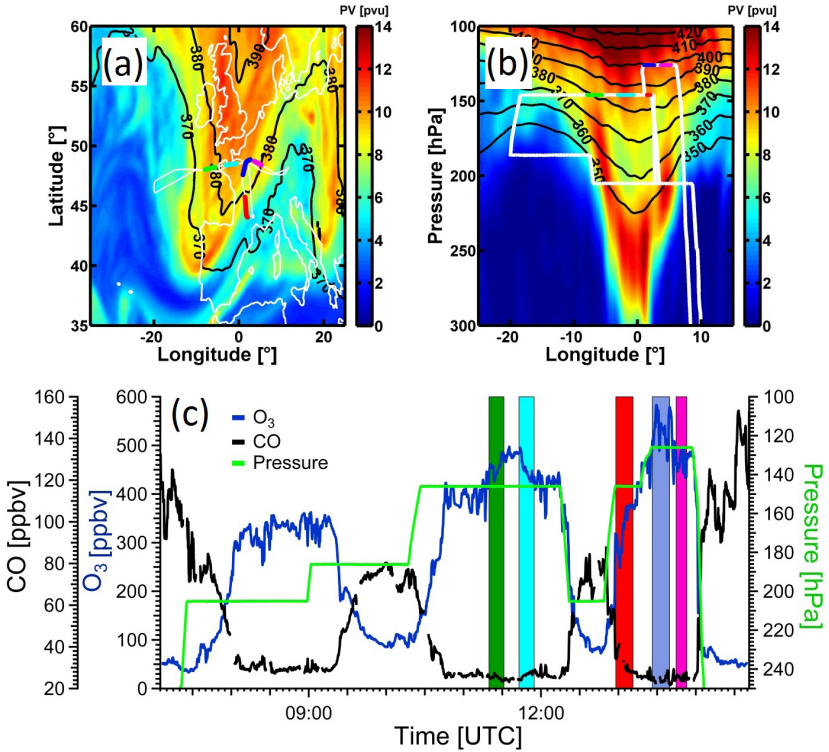

Figure 1. TACTS Flight 2 on 30 August 2012: **(a)** ECMWF data (15:00 UTC) at 150 hPa of potential vorticity (color) and potential temperature (black contour lines). The thick white line is the flight path of TACTS Flight 2, whereas different colors indicate flight legs with measured mixing lines (see Sect. 3). **(b)** Horizontal cross section of ECMWF potential vorticity data along 48.5° N equally to **(a)**. **(c)** Time series of CO (black), O_3 (blue) and Pressure (green). Data points which form mixing lines are marked in different colors according to panel **(a, b)**. The total uncertainty of CO and O_3 is mostly within the line thickness and therefore not shown (for individual error bars see Fig. 3).

ACPD
15, 34765–34812, 2015

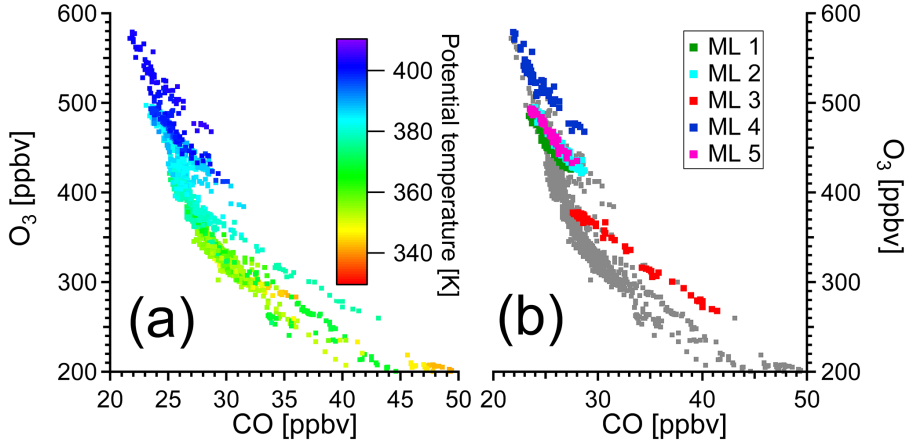

Figure 2. Stratospheric part of the CO–O_3-correlation for TACTS Flight 2 on 30 August 2012: **(a)** color-coded with measured potential temperature. **(b)** Mixing lines (ML) in different colors in accordance with Fig. 1. For error bars see Fig. 3.

ACPD
15, 34765–34812, 2015

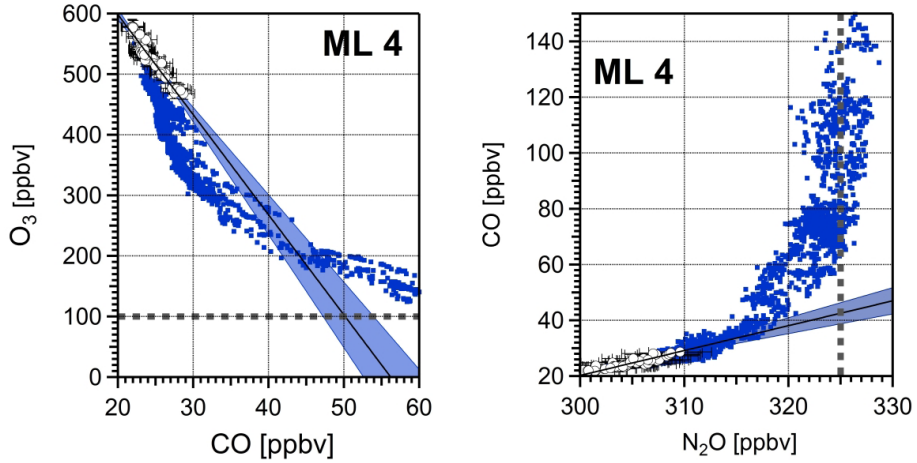

Figure 3. Linear fitting for ML 4 based on the FITEXY-routine described in Press et al. (1992). Blue dots: scatter plot of CO and O_3 (left), and N_2O and CO (right), respectively. White dots with black error bars: data points of ML 4 on the respective scatter plot. Solid black line: linear fit with confidence region (shaded area). Dotted lines: assumption of a tropospheric endmember of $R(O_3)_{Trop}$ = 100 ppbv (top) and $R(N_2O)_{Trop}$ = 325 ppbv (bottom).

ACPD
15, 34765–34812, 2015

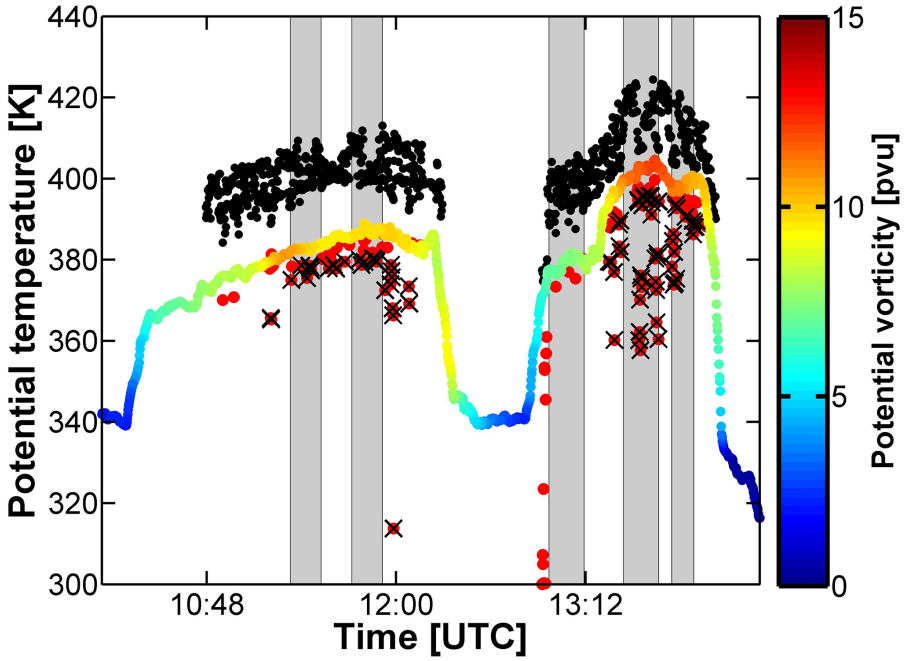

Figure 4. Solid line: time series of the measured potential temperature Θ for the second half of TACTS Flight 2 with PV as color (from ECMWF data). Black dots: maximum potential temperature along 50 days backward trajectories for all data points with Θ > 370 and PV > 4 pvu at the measurement location. Red dots: minimum potential temperature along 50 days backward trajectories for all data points with Θ > 370 K, PV > 4 pvu, and minimum Θ along the backwards trajectories is smaller as Θ at the measurement. Red dots with PV > 7.5 pvu and minimum Θ at least 5 K smaller as Θ at the measurement are marked with a black cross (cf. Fig. 5).

ACPD
15, 34765–34812, 2015

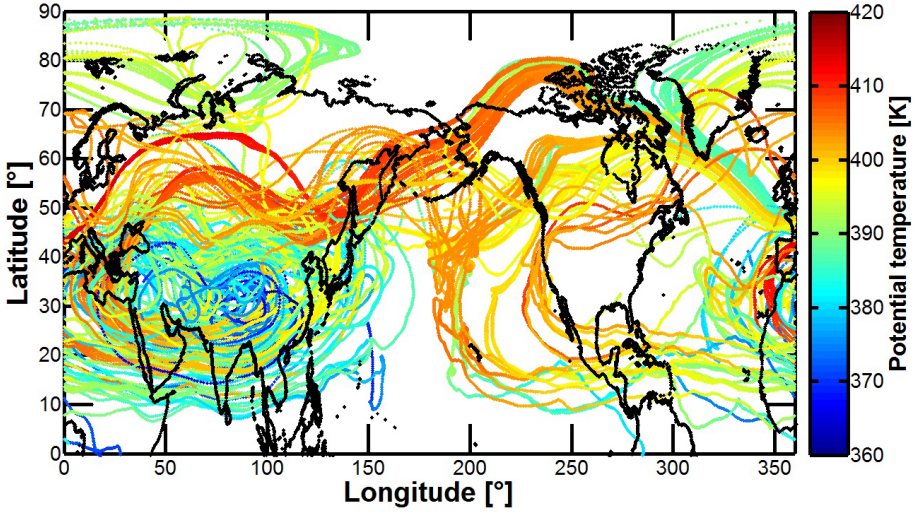

Figure 5. 50 day backward trajectories for all data points with $\Theta > 370$ K, PV > 7.5 pvu, and minimum Θ along the backwards trajectories is at least 5 K smaller as Θ at the measurement (cf. Fig. 4). Color: potential temperature along the backward trajecetories based on ERA-Interim reanalysis data.

ACPD
15, 34765–34812, 2015

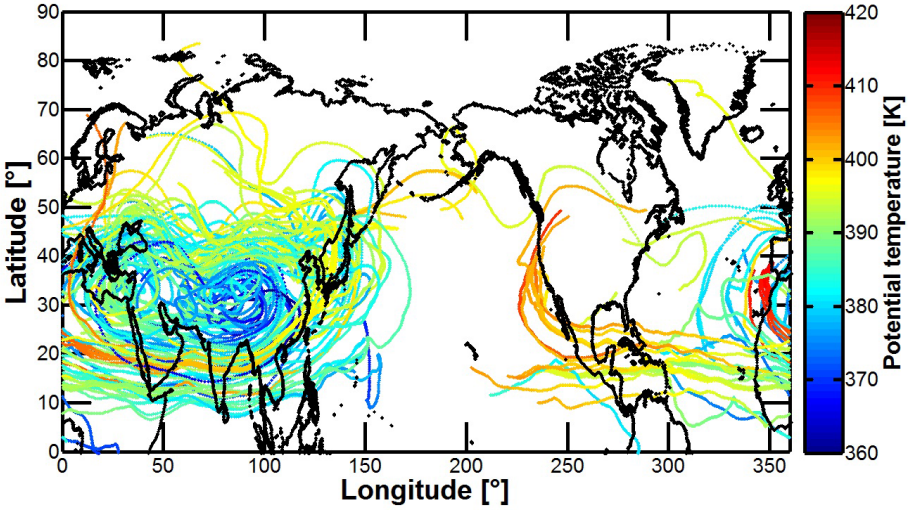

Figure 6. Pathway of same trajectories as shown in Fig. 5 for −50 days < t_{Tra} < −30 days.

ACPD
15, 34765–34812, 2015

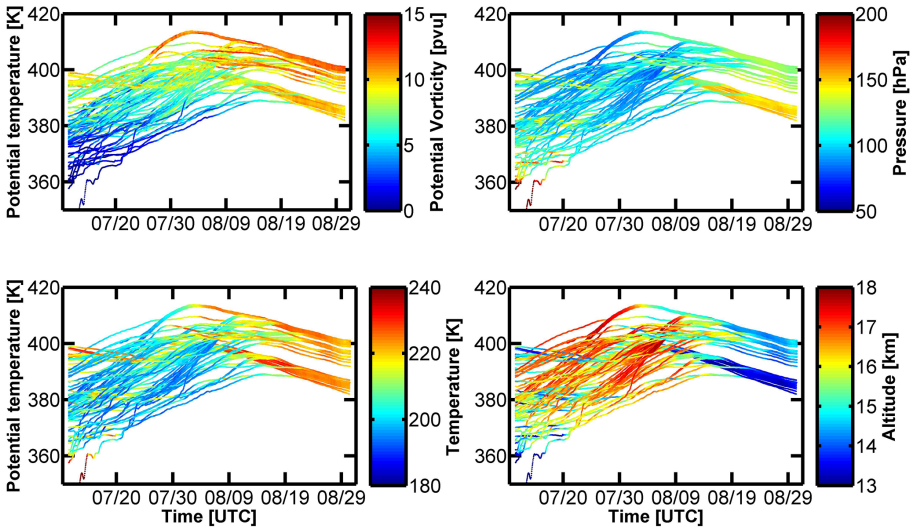

Figure 7. Potential temperature vs. time (in UTC) along the same 50 day backward trajectories as in Fig. 5 is shown. The color indicates the PV (top left), pressure (top right), temperature (bottom left), and altitude (bottom right) based on ERA-Interim reanalysis data.

ACPD
15, 34765–34812, 2015

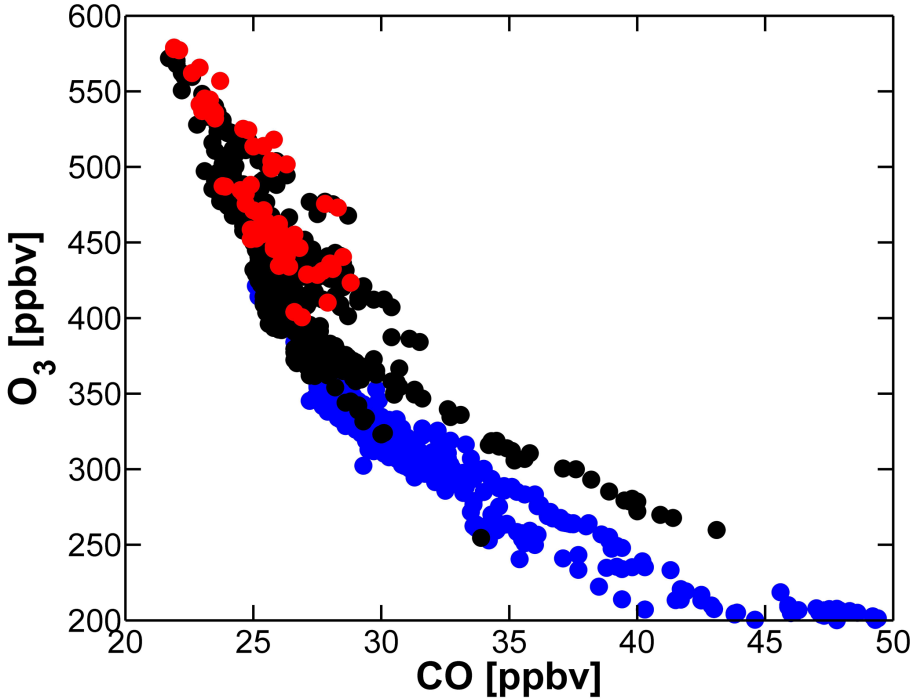

Figure 8. Blue: CO–O_3-correlation of TACTS Flight 2 (cf. Fig. 2). Black: data points that were measured at $\Theta > 370$ K and PV > 4 pvu. Red: data points which were measured at PV > 7.5 pvu und whose 50 day backward trajectories indicate an Θ_{min} at least 5 K below the measured Θ.

ACPD
15, 34765–34812, 2015

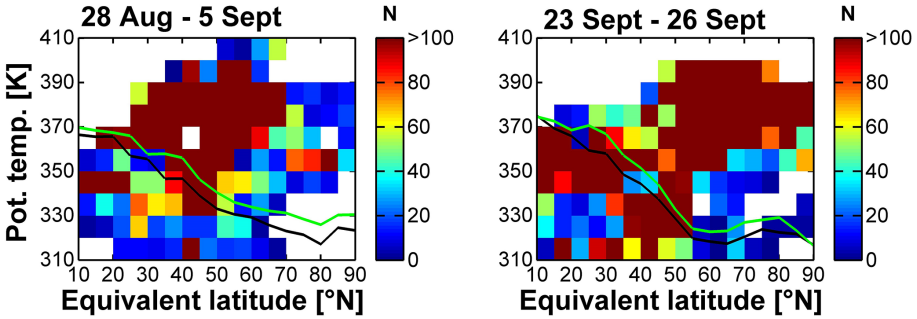

Figure 9. Data coverage (number of data points N in each bin) of TACTS 2012 in potential temperature Θ – equivalent latitude ϕ_{eq} – coordinates. Left: data coverage of the initial phase of TACTS from the 28 August to 5 September. Right: data coverage of the final phase of TACTS from the 23 to 26 September. The black and green line denotes the location of the dynamical (PV = 2 pvu) and thermal tropopause (WMO, 1957), respectively, for the associated time period from ECMWF data.

ACPD
15, 34765–34812, 2015

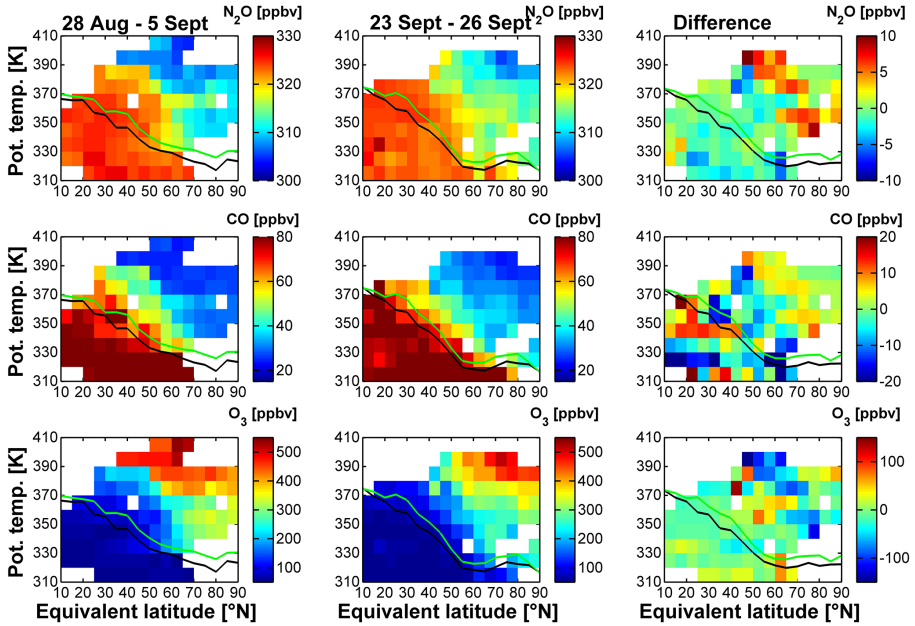

Figure 10. N_2O, CO, and O_3 distributions in potential temperature Θ – equivalent latitude ϕ_{eq} – coordinates for the TACTS 2012 campaign. Left: distributions for the initial phase of TACTS from the 28 August to 5 September. Center: distributions for the final phase of TACTS from the 23 to 26 September. Right: changes in the trace gas distributions during the TACTS 2012 campaign (final minus initial phase). The black and green line denotes the location of the dynamical (PV = 2 pvu) and thermal tropopause (WMO, 1957), respectively, for the associated time period from ECMWF data.

ACPD
15, 34765–34812, 2015

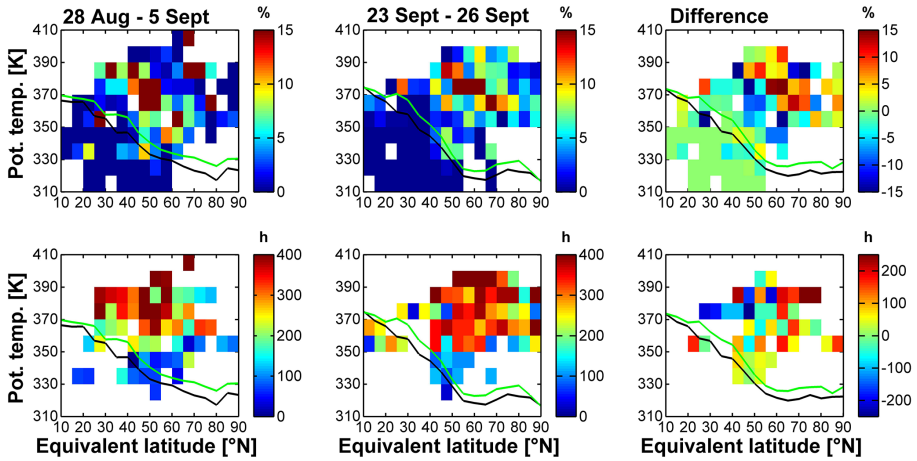

Figure 11. Same presentation as in Fig. 10 but with different color coding. Top: proportion of data points for which 50 backward trajectories calculated with CLaMS-TRAJ indicate an origin in the Asian summer monsoon anticyclone (Criterion: 20° N < TRA-latitude < 50° N, 40° E < TRA-longitude < 150° E and Tra-Θ > 360 K for $t = -30$ days). Bottom: mean residence time of trajectories in hours in the Asian monsoon anticyclone between $t = -50$ days and t_{meas} following the same criterion as in the middle array. Figures are filtered for bins with at least 10 data points.

ACPD
15, 34765–34812, 2015

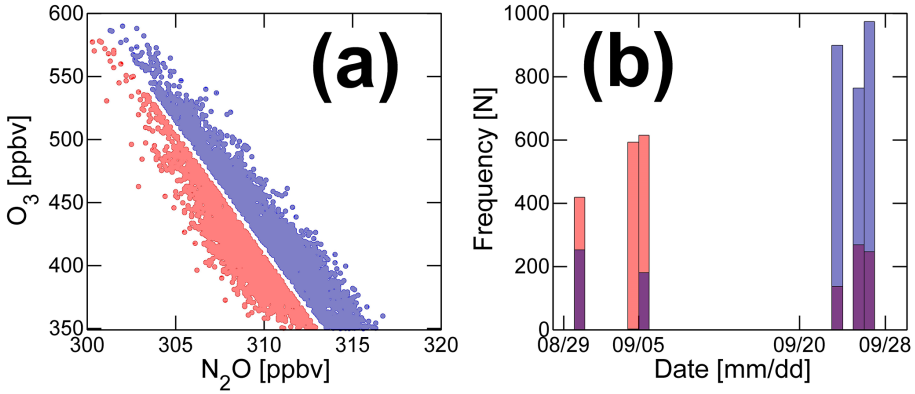

Figure 12. (a): N_2O–O_3-scatterplot of all data points during TACTS 2012 with $O_3 > 350$ ppbv divided into higher (blue) and lower (red) O_3 mixing ratios on N_2O isopleths based on a linear fit regression. **(b)**: histogram of the measurement date of the red and blue data points on the N_2O–O_3-scatterplot. Purple areas display the overlap of both histograms.

ACPD
15, 34765–34812, 2015

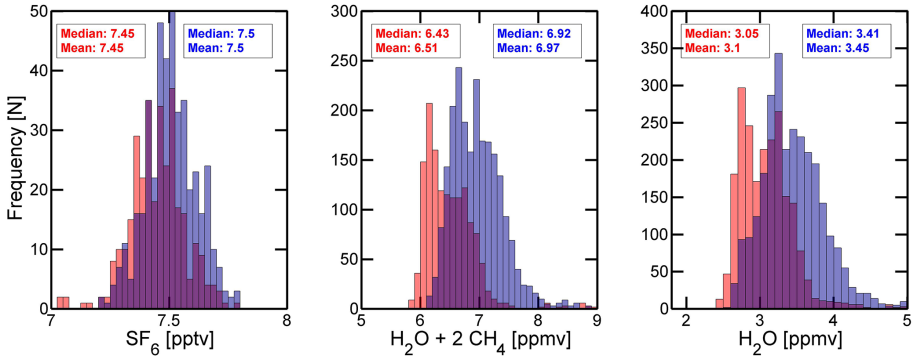

Figure 13. Histogram of trace gas mixing ratios of SF_6 (left), total water ($H_2O + 2CH_4$) (center) and H_2O of the red and blue data points on the N_2O–O_3-scatterplot in Fig. 12a. Purple areas display the overlap of both histograms.

ACPD
15, 34765–34812, 2015

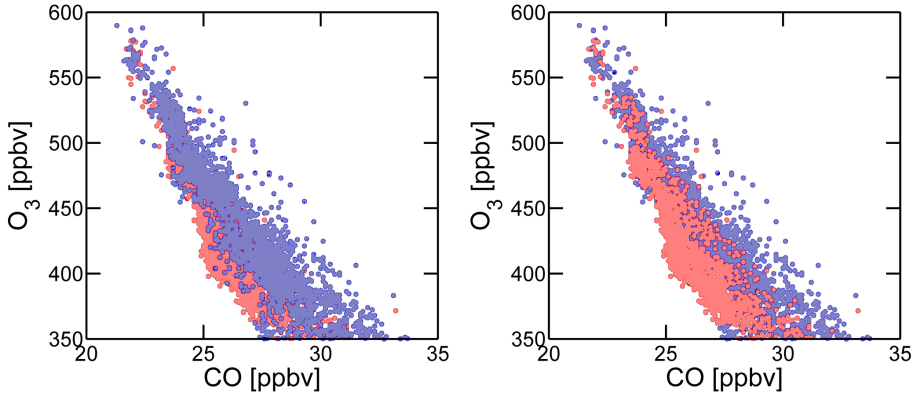

Figure 14. CO–O_3-scatterplot for the same data points as shown in the N_2O–O_3-scatterplot in Fig. 12a. Left: blue data points on top of red data points. Right: red data points on top of blue data points.

ACPD
15, 34765–34812, 2015